SUPPORTING INFORMATION

Chain Dynamics of Nascent Polypeptides

Emerging from the Ribosome

Jamie P. Ellis[†,1], Courtney K. Bakke[†,2], Robert N. Kirchdoerfer[3], Lisa M. Jungbauer[4],

Silvia Cavagnero[*,1]

Department of Chemistry, University of Wisconsin-Madison, 1101 University Avenue,

Madison, Wisconsin 53706, USA.

† These authors contributed equally to the work.

* To whom correspondence should be addressed.

[1] Department of Chemistry
University of Wisconsin-Madison
1101 University Avenue
Madison, WI 53706
Phone: 608-262-5430
FAX: 608-262-9918
Email: cavagnero@chem.wisc.edu

[2] Minnesota Dept. of Health
601 Robert St N
St. Paul, MN 55164

[3] The Scripps Research Institute
TPC-19
10550 N. Torrey Pines Rd.
La Jolla, CA 92037

[4] University of Illinois at Chicago
Dept. of Anatomy and Cell Biology
808 S. Wood St.
Chicago, IL 60612

Supporting Text

In order to further document the physical properties of nascent chains, ribosome and chaperones, a few additional types of biophysical characterization, not explicitly shown in the main text, were performed.

The gel electrophoresis analysis in the absence/presence of puromycin (see main article, Fig. 1D) was extended to additional apoMb nascent chains to demonstrate that they are predominantly ribosome-bound (Supp. Fig. 1).

Chaperones other than DnaK and trigger factor may be present in the transcription-translation mixture and resuspended ribosomes and possibly interact with nascent chains. Given that these interactions may affect the observed nascent chain dynamics it is important to test for the presence of additional chaperones and co-chaperones. Therefore, in addition to DnaK and TF, discussed in the main text of the article, we tested for the presence of SecB and DnaJ in the cell-free extract and resuspended ribosome solutions (Supp. Fig. 2). We found no evidence for the presence of DnaJ in either medium, while we detected SecB (≥ 0.8 μM) only in the cell-free extract but not in the resuspended ribosome-nascent chains (RNCs).

The polar/nonpolar character of the globular protein apoMb and the natively unfolded protein PIR_{90} was assessed at the amino acid-specific level (Supp. Fig. 3, panel a). PIR_{90} is very hydrophilic and has fewer aromatic side chains than apoMb. Additionally, the probability scores (Fig. 3, panel b,) for the binding of DnaK to the PIR_{90} protein sequence are much lower than for apoMb (*1*). The plots are in full agreement with the experimental results from immunoblotting, which show that the amounts of chaperones associated with PIR_{90} are small. The plot in Supporting Figure 3 is also consistent with the

dynamic fluorescence depolarization data, which show that ribosome-bound nascent PIR$_{90}$ is more flexible and less compact than ribosome-bound nascent apoMb.

Supporting Figure 4 illustrates the steady-state anisotropy of apoMb RNCs of increasing length. The data show that the average depolarization provided by the steady-state methodology is dominated by the tumbling of the ribosome (apparent molecular weight ca. 2.5 MDa), responsible for the extremely slow global tumbling of the RNC complex. Such tumbling occurs on a timescale much slower than the BODIPY-FL fluorophore lifetime, leading to an observed steady-state anisotropy fairly close to its maximum observable value (i.e., the fundamental anisotropy of the immobilized BODIPY-FL fluorophore, r_0 = 0.37). The local 3-7 ns motions due to the nascent protein chain cannot be explicitly resolved by the steady-state technique due to its inability to discriminate individual motions sensed by the fluorophore within the large macromolecular complex. Supporting evidence for this statement is provided by the fact that the steady-state anisotropy of apoMb1-35 is the same as those of the longer chains (including full length apoMb), within experimental error. The time-resolved fluorescence depolarization approach (see main article) overcomes the above drawback of the steady-state technique.

To aid in our interpretations, we calculated the expected fraction of nascent polypeptides buried inside the ribosomal exit tunnel (Figure 1, panel b of the manuscript). The current figure for the manuscript applies the common assumption of a ca. 100 Å-long tunnel (e.g. (*2*)). A more recent alternative definition of the ribosomal tunnel, quoting it as ca. 80 Å-long, (*3*), leads to slight changes, shown here in comparison with the original scheme (Supp. Fig. 5a and b). As shown in the figure, the 80 Å ribosomal tunnel definition places apoMb$_{57}$ out of the tunnel by a few amino acids, in case of a fully α-helical C terminus.

As shown in Supporting Figure 6, additional evidence supports the fact that the ribosomes are well behaved in solution by transmission electron microscopy (EM). The figure shows that both before and after purification (via ultracentrifugation followed by resuspension) ribosomes can be identified as approximately round species. This result applies under the diluted conditions required for EM data collection. We reproducibly identify neither polysomes nor irreversible large-scale aggregates in the samples, except for occasional higher order aggregates of unknown origin in the cell-free reaction mixtures.

Finally, we provide (A) the sequences for the deoxyoligonucleotides applied for directed mRNA cleavage and (B) the methods for simulating the expected apparent rotational correlation times of prolate ellipsoids starting from dynamic fluorescence depolarization data.

Supporting Methods

Oligonucleotide design for the isolation of ribosome-bound nascent chains.

Expression was carried out in the presence of a designed oligodeoxynucleotide with a sequence complementary to the desired mRNA cleavage site (*4*). Nascent chains were protected from tmRNA-mediated tagging and release from the ribosome by addition of an anti-ssrA oligonucleotide (*5*). The following oligonucleotides were used for generating the ribosome-bound nascent protein chains listed in the manuscript (final concentration 0.15 μg/μl):

5'- TTTAGCCCAAACATGCAGAACCAGCTGCCATTCACCTT -3', ApoMb$_{16}$;

5'- AGATTTGAACAGTCGAATCAAGATGTCCTGACCATGAC-3', ApoMb$_{35}$;

5'-AGCTTTCATTTCAGCTTCAGTTTTCAGATGTTTGAAAC-3', ApoMb$_{57}$;

5'-GCAAGCGGTTTGAGCTCAGCTTCATGATGCCCTTTTTT-3', ApoMb$_{89}$;

5'-ACCGAAGTCACCTGGATGTCTAGAATGCAGAACATGGA-3', ApoMb$_{124}$;

5'- ACCCTGGTAACCCAGTTCTTTGTACTTAGCAGCGATAT-3', ApoMb$_{153}$;

5'-GTGGTGGTGGTGGTGGTGCTCGAGTGCGGCCGCAAGCT-3', PIR$_{90}$;

5'- TTAAGCTGCTAAAGCGTAGTTTTCGTCGTTTGCGACTA-3', anti-ssrA oligonucleotide.

Testing for the presence of SecB and DnaJ by gel electrophoresis and Western blotting. As described in the article, the cell-free proteins were separated by SDS-PAGE (12% tris-glycine polyacrylamide gels) and transferred to a PVDF membrane. The membrane was probed with either rabbit anti-DnaJ (Stressgen) or anti-SecB polyclonal antibodies (gift of L. Randall). Goat anti-mouse alkaline phosphatase conjugates (Novagen) were used as secondary antibodies. Protein-antibody complexes were detected by chemiluminescence (CDP-Star$^{®}$ substrate, Novagen). Band intensities were compared to those of purified DnaJ or SecB standards of known concentration.

Steady-state anisotropy data collection. Steady-state data were obtained using a PC1 spectrofluorimeter (ISS) equipped with calcite prism polarizers (λ_{ex} = 485 nm, λ_{em} = 510-540 nm with an HP525BP30M filter, Chroma). The data in Supporting Figure 4 show the average of 2 to 5 independent experiments. The G factor was measured once for each experimental set and applied after data collection and background subtraction (*6*).

Calculation of expected rotational correlation times for different molecular geometries. The calculations described here were employed to compute the values required to generate Figure 7 of the main manuscript. ApoMb-derived polypeptides of 1-180 amino acids were modeled as either compact spherical structures, prolate ellipsoids with a defined axial ratio (ρ=3.5) and fully extended rigid polypeptides with an axial ratio increasing with chain length.

The simulations of spheres were done by computing rotational correlation times (τ_{SPHERE}) from the expected rotational diffusion coefficient, D_{SPHERE}, according to

$$D_{SPHERE} = \frac{RT}{6\eta V_h} \qquad \text{and} \qquad \tau_{SPHERE} = (6D_{SPHERE})^{-1}, \tag{1}$$

where R is the universal gas constant, T is the temperature (293 K), η is the viscosity (in mPa s), and V_h is the hydrated polypeptide volume, computed considering that a standard peptide dry volume of 0.75 ml/g contains 0.2 ml of H_2O/g of peptide (*6*). Estimates of D_{SPHERE} were obtained for the two limiting viscosities of free BODIPY and full-length apoMb, in RNC solutions. Experimental viscosities for the above molecules were obtained from dynamic fluorescence depolarization (which yields apparent τ_C) via relation 1, assuming spherical shape. The experimental BODIPY depolarization data fit best to two motions. The first one is identical to the τ_C of free BODIPY in water within error. The second slower motion, indicative of nonspecific binding and/or aggregation, was ignored

for the purpose of the present calculations (*7*). The viscosities of BODIPY and apoMb are significantly different, as described in the text of the article, primarily due to size-dependent crowding effects.

The simulations of prolate ellipsoids were done by computing the parallel and perpendicular components of the rotational diffusion coefficient according to

$$D_{\parallel} = \frac{3\rho \times (\rho - S)}{2 \times (\rho^2 - 1)} \times D_{SPHERE} \qquad \text{and} \qquad D_{\perp} = \frac{3\rho \times [(2\rho - 1)S - \rho]}{2 \times (\rho^4 - 1)} \times D_{SPHERE} \qquad (2)$$

with S equal to

$$S = (\rho^2 - 1)^{-\frac{1}{2}} \ln\left[\rho + (\rho^2 - 1)^{\frac{1}{2}}\right] \; , \qquad (3)$$

where ρ is the aspect ratio, i.e., the ratio of the long and short ellipsoid radii, The absorption and emission transition dipole moments of the fluorophore were assumed to be approximately parallel and randomly oriented relative to the ellipsoid axes. The components of the rotational diffusion coefficient were then converted to one experimentally observable correlation time, the harmonic mean of the motions, τ_H, according to,

$$\tau_1 = (D_{\parallel} + 5D_{\perp})^{-1} \quad , \quad \tau_2 = (4D_{\parallel} + 2D_{\perp})^{-1} \quad \text{and} \qquad \tau_3 = (6D_{\perp})^{-1} \quad , \qquad (4)$$

where

$$\tau_H = \left(\frac{0.4}{\tau_1} + \frac{0.4}{\tau_2} + \frac{0.2}{\tau_3}\right)^{-1} . \qquad (5)$$

The calculations of τ_c for fully extended chains were carried out by regarding the long axis of the prolate ellipsoid as corresponding to a fully extended peptide backbone (i.e., 3.4 Å/residue). The short axis was computed as the sum of the average peptide backbone width (estimated to be 2.4 Å) and twice the average length of the amino acid side chain in proteins, where each naturally occurring residue was weighted according to

its frequency of occurrence in the crystallographic database (*8*). Amino acid side chain lengths were calculated as the summation of the distance between C_α and the center of mass for the side chain with the radius of gyration, R_g, of the side chain. (*9*)

Acknowledgments

Supporting Figure Legends

Supporting Figure 1. Gel electrophoresis of resuspended ribosomes carrying nascent chains (wild-type strain). Peptidyl-tRNAs were resolved on an acidic gels (pH 5.7), to minimize hydrolysis of the peptidyl-tRNA ester bond. Samples are shown both before (odd lanes) and after (even lanes) treatment with puromycin. Gel images were taken at different gain values to optimize sample detection.

Supporting Figure 2. Western blots testing for the presence of SecB (a) and DnaJ (b) using either anti-SecB or anti-DnaJ antibodies. Cell-free expression was performed in both wild-type (WT) and Δtig cell extracts. Both cell-free extracts and resuspended ApoMb$_{153}$ RNCs were analyzed.

Supporting Figure 3. a) Nonpolar character of apoMb (black) and PIR$_{90}$ (grey), evaluated as mean buried surface area, computed as described (*10*). Aromatic residues (Phe, Trp, Tyr) are highlighted by stars. **b)** Probability scores for the binding of DnaK to the apoMb protein sequence using a known DnaK prediction algorithm (*1*). Negative scores denote higher binding probabilties. The *residue number* label denotes the central amino acid of each computed segment of primary structure.
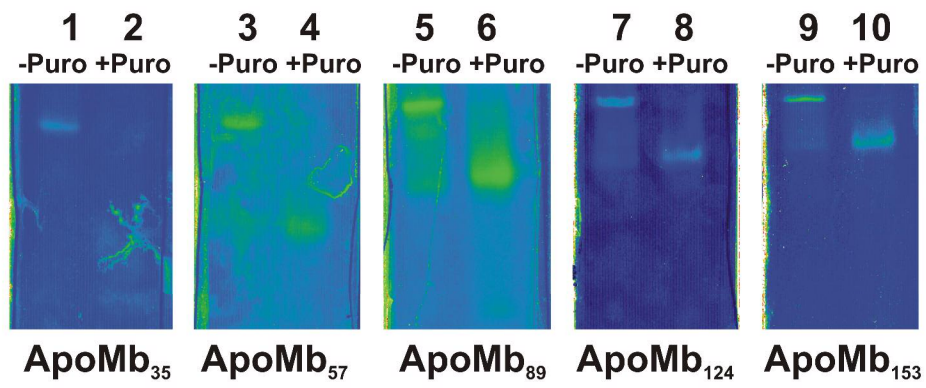
Supporting Figure 4. Steady-state fluorescence anisotropy analysis of apoMb RNCs generated in the wild-type *E. coli* cell-free system.

Supporting Figure 5. Comparison of the expected fraction of nascent polypeptides buried inside the ribosomal exit tunnel for two estimates of the tunnel length**:** a) 100 Å and b) 80 Å, assuming either an α-helical or extended β-strand limiting nascent chain conformations.
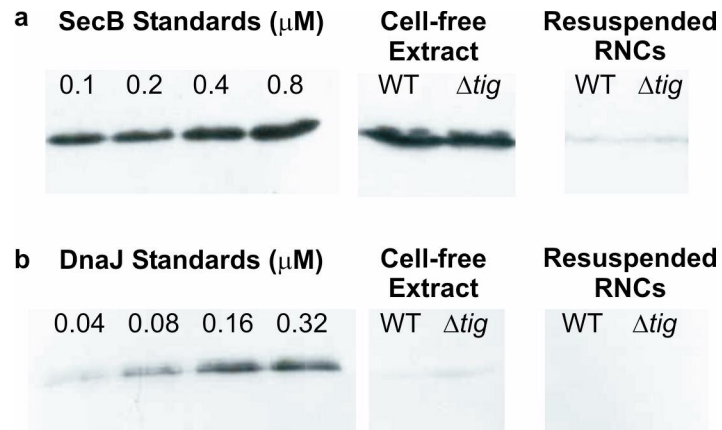

Supporting Figure 6. Transmission EM micrographs of *E. coli* ribosomes carrying the apoMb$_{124}$ nascent chain. Selected ribosomes are highlighted by arrows. Samples are as follows: A) trigger factor-deficient system, resuspended ribosomes after ultracentrifugation; B) trigger factor deficient system, unpurified cell-free expression mixture; C) wild-type system, resuspended ribosomes after ultracentrifugation; D) wild-type system, unpurified cell-free expression mixture. In both of the unpurified systems, aggregates were found to be sparingly present (not pictured). These aggregates occasionally include species of the approximate size of the ribosome.
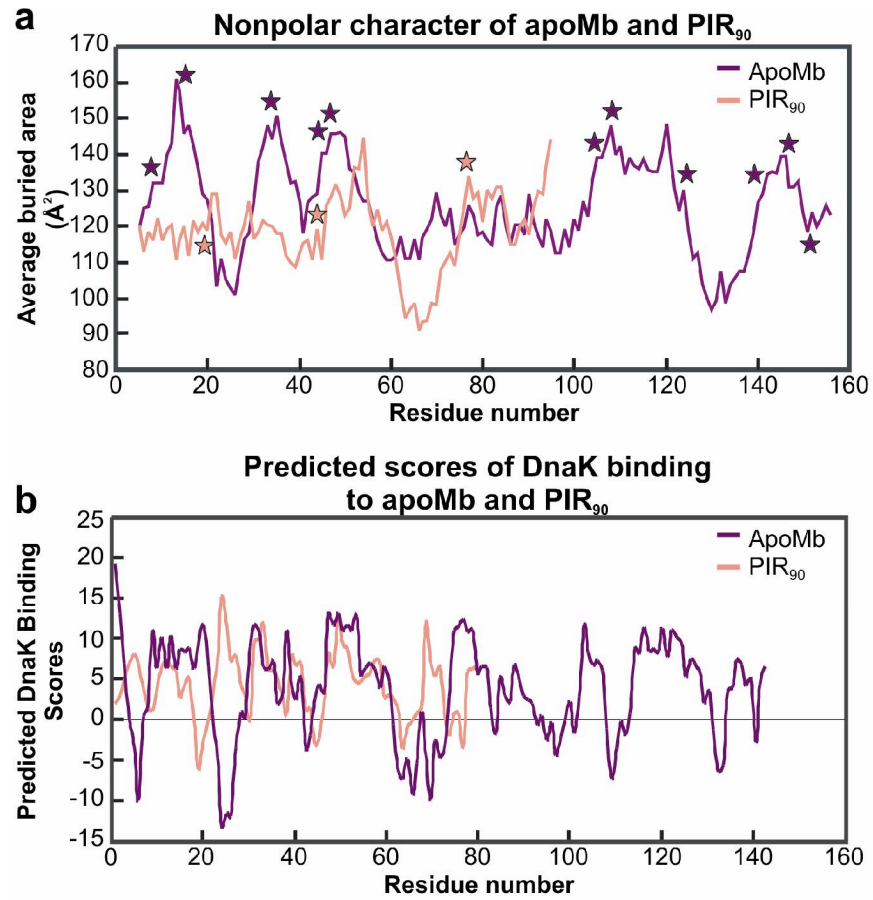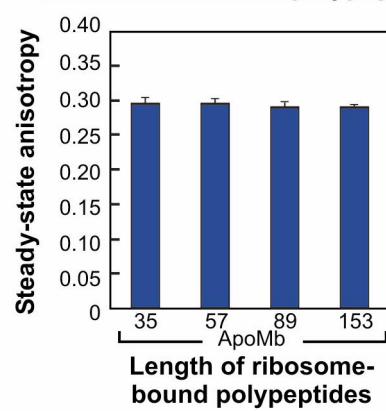
Supporting Figure 1

Supporting Figure 2

a **SecB Standards (μM)** **Cell-free Extract** **Resuspended RNCs**

0.1   0.2   0.4   0.8   WT   Δ*tig*   WT   Δ*tig*

b **DnaJ Standards (μM)** **Cell-free Extract** **Resuspended RNCs**

0.04 0.08 0.16 0.32   WT   Δ*tig*   WT   Δ*tig*

a Nonpolar character of apoMb and PIR$_{90}$

b Predicted scores of DnaK binding to apoMb and PIR$_{90}$

Supporting Figure 4

Steady-state fluorescence anisotropy of ribosome-bound polypeptides

Length of ribosome-bound polypeptides

a **Fraction of chains buried in the ribosomal tunnel (100 Å)**

b **Fraction of chains buried in the ribosomal tunnel (80 Å)**
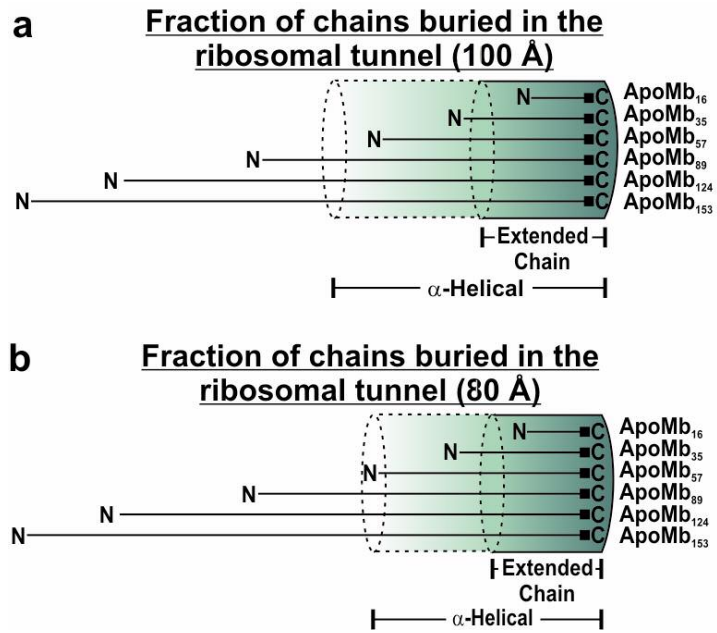
Supporting Figure 6
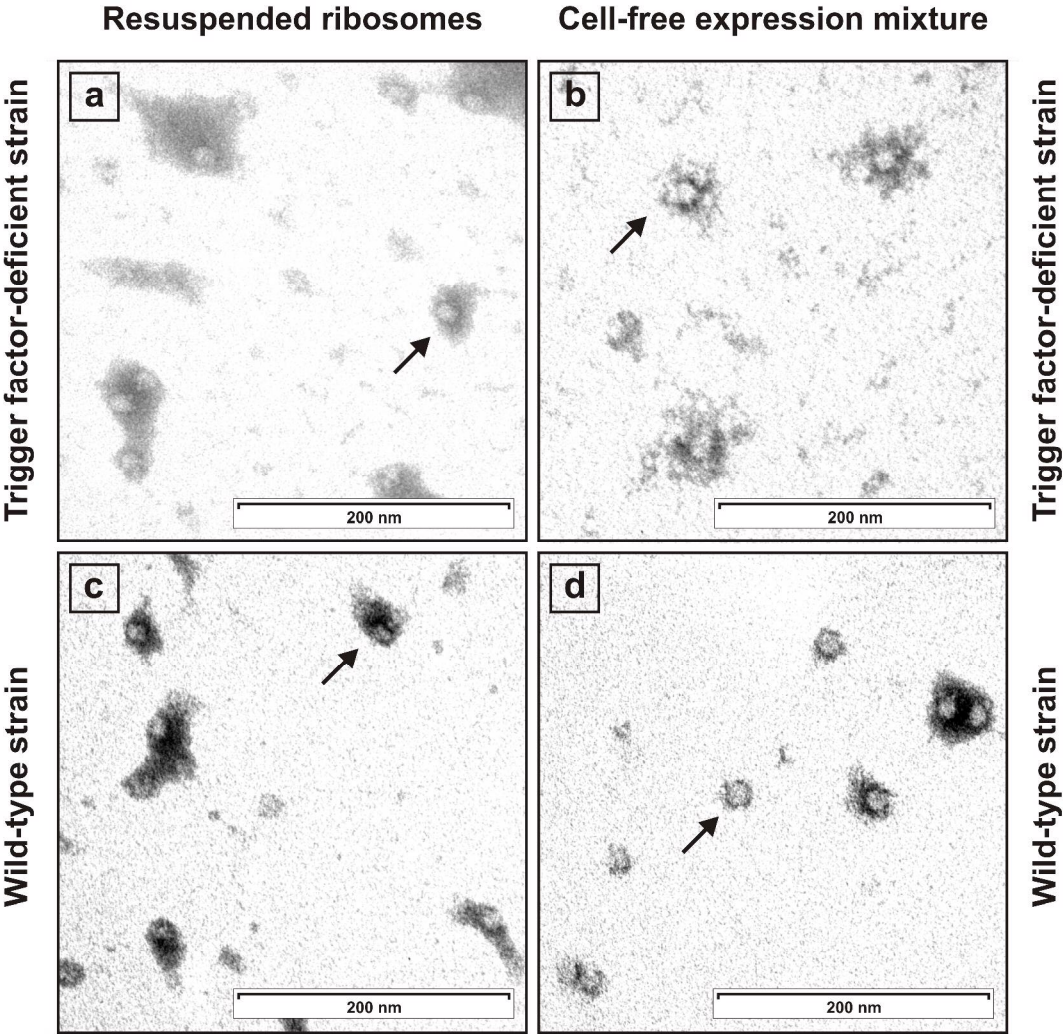
Supporting References

(1)   Rudiger, S., Germeroth, L., Schneider-Mergener, J., and Bukau, B. (1997) Substrate specificity of the DnaK chaperone determined by screening cellulose-bound peptide libraries. *EMBO J. 16*, 1501–1507.

(2)   Nissen, P., Hansen, J., et al. (2000) The structural basis of ribosome activity in peptide bond synthesis. *Science 289*, 920–930.

(3)   Voss, N. R., Gerstein, M., Steitz, T. A., and Moore, P. B. (2006) The Geometry of the Ribosomal Polypeptide Exit Tunnel. *J. Mol. Biol. 360*, 893–906.

(4)   Behrmann, M., Koch, H. G., et al. (1998) Requirements for the translocation of elongation-arrested, ribosome-associated OmpA across the plasma membrane of *E coli. J. Biol. Chem. 273*, 13898–13904.

(5)   Hanes, J., and Pluckthun, A. (1997) *In vitro* selection and evolution of functional proteins by using ribosome display. *Proc. Natl. Acad. Sci. U. S. A. 94*, 4937–4942.

(6)   Lakowicz, J. R. (2006) in *Principles of Fluorescence Spectroscopy*, Springer Science, New York.

(7)   Verkman, A. S. (2002) Solute and macromolecule diffusion in cellular aqueous compartments. *Trends Biochem. Sci. 27*, 27–33.

(8)   McCaldon, P., and Argos, P. (1988) Oligopeptide biases in protein sequences and their use in predicting protein coding regions in nucleotide sequences. *Proteins 4*, 99–122.

(9)   Levitt, M. (1976) A simplified representation of protein conformations for rapid simulation of protein folding. *J. Mol. Biol. 104*, 59–107.

(10)   Rose, G. D., Geselowitz, A. R., et al. (1985) Hydrophobicity of Amino-Acid Residues in Globular-Proteins. *Science 229*, 834–838.